

# Molecular-dynamics simulation of polyimide matrix pre-crystallization near the surface of a single-walled carbon nanotube†

Cite this: *RSC Adv.*, 2014, 4, 830

Sergey V. Larin,<sup>a</sup> Stanislav G. Falkovich,<sup>a</sup> Victor M. Nazarychev,<sup>a</sup> Andrey A. Gurtovenko,<sup>ab</sup> Alexey V. Lyulin<sup>c</sup> and Sergey V. Lyulin<sup>\*ab</sup>

Polyimide-based composite materials with a single-walled carbon nanotube as filler were studied by means of extensive fully-atomistic molecular-dynamics simulations. Polyimides (PI) were considered based on 1,3-bis-(3',4-dicarboxyphenoxy)-benzene (dianhydride R) and various types of diamines: 4,4'-bis-(4''-aminophenoxy)-diphenylsulfone (diamine BAPS) and 4,4'-bis-(4''-aminophenoxy)-diphenyl (diamine BAPB). The influence of the chemical structure of the polyimides on the microstructure of the composite matrix near the filler surface and away from it was investigated. The formation of subsurface layers close to the nanotube surface was found for all composites considered. In the case of R-BAPB-based composites, the formation of an organized structure was shown that could be the initial stage of the matrix crystallization process observed experimentally. Similar structural features were not observed in the R-BAPS composites. Carbon nanotubes induce the elongation of R-BAPB chains in composites whereas R-BAPS chains become more compact similar to what is observed for EXTEM™ polyimide. It was shown that electrostatic interactions do not influence the microstructure of composites but slow down significantly the dynamics of PI chains in composites.

Received 11th September 2013  
Accepted 8th November 2013

DOI: 10.1039/c3ra45010d

www.rsc.org/advances

## Introduction

In recent years, polymer composite materials (PCM) have found wider applications in various areas, including mechanical engineering, the aerospace and automotive industries.<sup>1-3</sup> Having low specific weight compared to, for instance, metals, PCMs may feature a good mechanical performance, increased wear resistance, chemical stability, heat and thermal resistance *etc.*<sup>1,2</sup> A wide variety of polymers may be used as matrices for PCMs.<sup>4-6</sup> These polymers can have a relatively simple or rather complicated molecular structure. However, even small changes in the polymer chemical structure can lead to a significant change in final PCM properties.<sup>1,2</sup>

High heat resistance is a parameter of crucial importance in many PCM applications which makes it possible to use PCMs at elevated temperatures without loss of their properties (*e.g.* mechanical ones). To produce such kind of PCMs, aromatic

polyimides (PI) which represent a class of thermally resistant polymers are widely used in modern industry.<sup>7-10</sup>

PI-based composites are rather difficult to produce since many polymers of this class do not dissolve in the majority of solvents whereas temperatures exceeding the glass-transition point might cause their active thermal degradation. A traditional technique to form PI-based PCMs is to polymerize the mixture initially containing a filler.<sup>11-14</sup> The drawbacks of this method include its overall labor intensity and an enhanced environmental hazard, particularly when using nanofillers which may be released into the environment together with the solvent waste.

Recent years have seen the development of PIs which are both thermally resistant and thermoplastic, *i.e.* they become viscoelastic without any thermal degradation. This property enables the formation of PCMs based on such PIs using melt technology.<sup>4,15-17</sup>

Recently a range of thermoplastic PIs have been synthesized in the Institute of Macromolecular Compounds of the Russian Academy of Sciences. These PIs can be processed using the melting technology, and have a big potential in terms of their application as thermoplastic matrices for PCM.<sup>15,17</sup> In particular, polyimides have been synthesized which are based on 1,3-bis-(3',4-dicarboxyphenoxy)-benzene (dianhydride R) and various types of diamines: 4,4'-bis-(4''-aminophenoxy)-diphenylsulfone (diamine BAPS) and 4,4'-bis-(4''-aminophenoxy)-diphenyl

<sup>a</sup>Institute of Macromolecular Compounds, Russian Academy of Sciences, Bol'shoi pr. 31 (V.O.), St. Petersburg, 199004 Russia. E-mail: s.v.lyulin@gmail.com; Fax: +7 (812) 3286869; Tel: +7 (812) 3285601

<sup>b</sup>Department of Physics, St. Petersburg State University, Ul'yanovskaya str. 1, Petrodvorets, St. Petersburg, 198504 Russia

<sup>c</sup>Theory of Polymers and Soft Matter Group, Technische Universiteit Eindhoven, PO Box 513, 5600 MB Eindhoven, The Netherlands

† Electronic supplementary information (ESI) available. See DOI: 10.1039/c3ra45010d

(diamine BAPB). The chemical structures of the repeating units of these PIs are shown in Fig. 1.

The major structural difference of these PIs is the presence of an additional sulfone hinge group in the R-BAPS diamine fragment compared to the R-BAPB one. Such a small change of the chemical structure enhances the flexibility of the R-BAPS polymer chain compared to the R-BAPB and alters its physical properties. The persistence lengths  $l_p$  calculated using the virtual bonds formalism equal 11.7 Å and 10.1 Å in the case of R-BAPB and R-BAPS, respectively (difference is ~10%).<sup>18,19</sup> Despite higher flexibility, R-BAPS is characterized by higher glass-transition temperature  $T_g$  which is ~490 K, and for R-BAPB ~477 K.<sup>15,17–20</sup> The most probable reason of increased  $T_g$  of R-BAPS is high polarity of the sulphone group, as was shown in our previous studies,<sup>18,20</sup> which also influences the properties of the R-BAPS polyimide. Also the R-BAPB is semicrystallizable with the melting point of  $T_m = 593$  K,<sup>15,18,20</sup> whereas the R-BAPS is an amorphous one.

R-BAPB and R-BAPS can be utilized as matrices to form PCMs with various nanofillers such as montmorillonite particles, carbon nanofibers and nanotubes.<sup>15,17,21–25</sup> The materials produced feature enhanced mechanical properties and higher heat resistance than filler-free bulk PIs. Therefore, it is rather important to clarify the impact of the chemical-structure modification on the final properties of the PI-based PCMs.

The addition of nanosized fillers in PCMs has considerable practical effects due to the fillers high specific surface.<sup>4,26–35</sup> Among all types of nanofillers, it is carbon nanotubes (CNT) that attract greatest attention due to their exceptional

mechanical,<sup>36</sup> electrical<sup>37</sup> and thermophysical properties.<sup>33,38</sup> The use of CNT as fillers for the production of nanocomposites may lead to considerable changes in the material performance compared to the original polymer matrix.<sup>35</sup>

An important feature of the interaction between CNTs and the polymer is their ability to act as nucleation agents causing the matrix crystallization in the PCMs.<sup>5</sup> Such a behavior has been established in the PCMs based on polyethylene,<sup>39–41</sup> polyacrylonitrile,<sup>42</sup> aromatic PIs,<sup>43</sup> including R-BAPB.<sup>21–25</sup>

The fact is of interest that CNT may even induce the crystallization of such polymers which do not crystallize under normal conditions and are amorphous, such as, for example, the ODP-A-P3 polyimide.<sup>43</sup> Polymer crystallization in a nanocomposite may significantly affect its mechanical and thermophysical properties, which has to be taken into account when developing new PCMs.<sup>5,44</sup>

The study of the structure and properties of PCM in the interface area between the matrix and the filler is essential to explain molecular mechanisms for altering the material properties following the embedding of the filler. Furthermore, investigation of the interrelation between the subsurface layer structure and both polymer matrix and nanofiller structure enables the forecasting of the end material properties, which is of high importance for the development and formation of new PCMs.

In order to address this issue, atomistic molecular dynamics (MD) simulation methods are successfully employed.<sup>45–47</sup> The use of MD in combination with detailed atomistic models describing the polymers and nanofillers makes it possible to

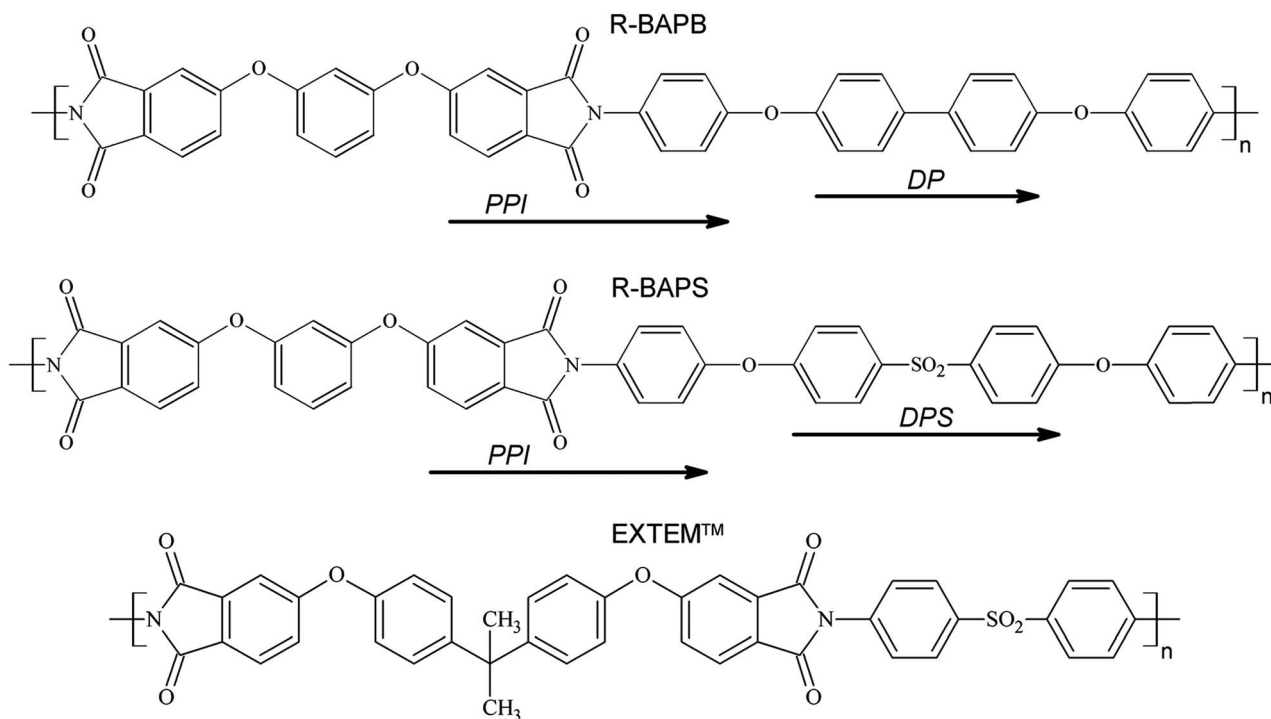


Fig. 1 Chemical structures of the repeating units of thermoplastic heat-resistant polyimides R-BAPB (top), R-BAPS (middle), and EXTEM™ (bottom). Arrows indicate phenylphthalimide (PPI), diphenyl (DP), and diphenylsulphone (DPS) fragments of PI monomer units that were chosen to calculate orientational characteristics as described below.

study the structure and properties of the PCMs on the atomistic scale, and establish mechanisms influencing them, as well as the correlation between the polymer matrix chemical structure specifics and changes occurring after the filler embedding.

This paper aims at investigating, by using the MD simulations, the changes taking place in the polyimide matrix structure when forming a composite material with a single-walled CNT as filler, both near the CNT surface and at a certain distance from it. The nature of the changes taking place in the matrix is mainly studied for two types of PI (R-BAPB and R-BAPS) which differ in the chain flexibility, geometric configuration of the units and the presence of polar groups. The influence of the electrostatic interactions in the computer simulation on the nature of the changes taking place in the polymer matrix has been clarified.

The rest of the paper is organized as follows. The second section contains the description of the model used and the simulation techniques followed by the presentation of the simulation results and their discussion. The final part provides a summary of the results obtained supported by the relevant conclusions.

## Simulation model and technique

In this paper we present MD simulations of nanocomposites based on the heat-resistant PI reinforced by a single-walled CNT with the use of all-atom representation. The simulations have been performed using the Gromacs computational package<sup>48,49</sup> and the Gromos53a6 force field<sup>50</sup> which were successfully used for bulk PI simulations.<sup>18–20,51</sup>

The cubic cell with periodic boundary conditions for each of the systems studied contained 27 chains of polyimides with a polymerization degree of  $n_p = 8$ , and one single-walled CNT. This  $n_p$  for R-BAPS and R-BAPB polyimides corresponds to the molecular weight  $M_n \sim 6.4 \text{ kg mol}^{-1}$ , at which the transition to the “polymer mode” is observed from the molecular-weight dependence of the glass-transition temperature.<sup>17,18,20,51</sup> The contour length of a polymer chain with  $n_p = 8$  is 31.0 nm and 37.5 nm for R-BAPB and R-BAPS, respectively. At the same time the average gyration radius of the PI chains is 4.0 nm for R-BAPB and 2.9 nm for R-BAPS (at temperature of  $T = 600 \text{ K}$ ). Thus, the PI coils are able to fit the simulation cell.

The size of the CNT has been chosen so that in the simulation the mass fraction of the filler in the composite equals 3% corresponding to the mass fraction of the filler in the heat-resistant PI-based nanocomposites studied earlier experimentally.<sup>15,17,21–25</sup> In this case, the CNT length should be less than that of the periodic cell edge ( $L_{\text{box}} \sim 6 \text{ nm}$ ). The nanotube diameter has been chosen so as to prevent the polymer chains from penetrating into its inner void. As a result a single-walled CNT has been chosen consisting of 400 carbon atoms with chirality (5,5), diameter equals to 0.7 nm, and the length is 4.7 nm. To maintain the carbon atoms valence, hydrogen atoms were attached to the ends of the CNT. Therefore, the filler mass fraction and volume fraction in the simulated composites amounted to approx. 3%, and 1.5%, respectively.

The simulation was performed in the NpT ensemble. The system temperature and pressure were maintained at the required level using a Berendsen thermostat and a Berendsen barostat, respectively,<sup>52,53</sup> the time constants for which were taken as  $\tau_T = 0.1 \text{ ps}$  for the thermostat, and  $\tau_p = 0.5 \text{ ps}$  for the barostat.<sup>18–20,54</sup> To maintain the length of the bonds between the atoms, the LINCS algorithm was used.<sup>55</sup>

In spite of the fact that the Berendsen barostat leads to higher pressure fluctuations than more accurate Parrinello–Rahman barostat, both barostats give practically the same system density fluctuations and rather similar local polymer microstructures. This has been tested in the present study for PCMs based on R-BAPB and R-BAPS polyimides. Therefore, the Berendsen barostat was chosen to be used within the approach developed earlier for simulations of bulk PIs.<sup>20</sup>

Notably, accounting for the chemically validated atomic partial charges during the simulation may influence significantly the properties of the simulated systems, particularly when groups with high polarity are present in the compounds under study.<sup>18–20</sup> Nevertheless, when atomic partial charges are expected to be quite small, they do not have any visible impact on the calculated properties.<sup>56</sup> A number of previous studies describe the simulation results of the systems based on polystyrene<sup>56–60</sup> and polyethylene,<sup>61–72</sup> in the absence of electrostatic interactions. The data obtained in these papers on the polymer local structure, and its thermophysical and mechanical properties are consistent with the experimental data. Nonetheless, accounting for electrostatic interactions for heterocyclic polymers with a complicated molecular structure, such as PIs, is of crucial importance for the calculation of their macroscopic thermophysical properties.<sup>18,20</sup>

This paper presents the simulation of PCMs based on heat-resistant PIs both with and without electrostatic interactions (with zero atomic partial charges) accounted for. The atomic partial charges were calculated for the atoms of the PI chain fragments consisting of two repeating units (dimer) using the Hartree–Fock (HF) quantum chemical method and the basis set of wave functions 6-31G\*.<sup>20</sup> The geometry optimization of the dimers was followed by the calculation of the atomic partial charges using the Mullikan method. The quantum chemical calculations were carried out using the Firefly software package.<sup>73</sup> The simulation with the charges calculated using this method quantitatively reproduces the volumetric-thermal-expansion coefficient value of the bulk R-BAPS.<sup>20</sup> The values of the partial charges for both R-BAPB and R-BAPS polyimides are listed in the ESI.†

The electrostatic interaction energies were accounted for by the particle-mesh Ewald summation (PME) method.<sup>74,75</sup> The cutoff radius for the calculation of electrostatic interactions in real space equaled 1 nm, the mesh size for the integration in Fourier space being assumed to be equal to 0.12 nm.<sup>18–20</sup>

Generation of initial configuration of polymeric systems and their equilibration is a rather difficult task in any computer simulation. Reliable determination of the PCM properties, particularly in terms of its microstructure, is possible only when the systems are well-equilibrated. Both the system initial configuration generation and the subsequent equilibration

procedure are of significance. The complicity of the issue lies mainly in the fact that producing equilibrated polymeric samples requires the simulation within the time periods stretching the limits of computing capacities available at the modern computer development stage. The problem of obtaining an equilibrium configuration of polymeric systems was addressed as early as in the classic papers by Theodorou *et al.*<sup>64,76,77</sup> and other authors,<sup>45,78–82</sup> yet it has not been completely solved.

There exist several approaches to generate the nano-composite initial configuration. The simplest one is to produce a low-density system containing one or several not overlapping polymer chains (polymeric “gas”) followed by the system compression.<sup>18,83,84</sup> In this case, the initial configuration of PI can be created using coarse-grained models followed by the system conversion into an all-atom representation.<sup>47</sup> Another approach to create the initial configuration implies the use of the Amorphous Cell module of the commercial software package Accelrys Materials Studio,<sup>47,85–87</sup> however, this method has a number of drawbacks. In particular, the application of this method to generate the initial configurations for bulk aromatic polymer samples may lead to the occurrence of polymeric structure artifacts in the form of interlocking between the periodic parts of the repeating units.<sup>82,88</sup> To avoid such situations, the initial configuration is generated with the density significantly lower than the experimental one (polymer density about 10% of the experimental density value). After that the system is compressed with a high pressure of up to several thousand bar applied to achieve the experimental density, and additional simulation is performed to finally equilibrate the sample.

The generation of initial configuration and further equilibration are of crucial importance for the systems accommodating self-organization processes, such as crystallization. Crystallization is quite a lengthy process,<sup>41,89</sup> and often crystallization simulation is impossible, particularly using atomistic models. Therefore, in the majority of papers focusing on the modeling of crystalline polymers, the system initial configuration is artificially set in the crystal form.<sup>90–97</sup> The initial parameters of the cell are given on the basis of the crystallographic data available. These papers usually investigate the properties of crystals and processes related to their melting at increased temperatures.

So far, the simulation of crystallization process has been carried out only for polymers with a rather simple chemical structure, such as polyethylene<sup>65–72,89,98</sup> or polypropylene.<sup>95</sup> Notably, many papers offer simulations of relatively small systems consisting of one long<sup>66,67,71,72</sup> or several short<sup>65,98</sup> polymer chains in vacuum,<sup>65–67</sup> near the graphene<sup>72</sup> or CNT<sup>71,98</sup> surface. These papers point out the formation of crystalline structures with the polymer chain lying along the surface making up layered crystal-like structures.<sup>71,72,98</sup>

Within this paper, the generation of the system initial configuration and its preliminary equilibration was performed pursuant to the procedure which was suggested and verified using experimental data in our previous studies devoted to simulation of bulk PIs.<sup>18–20,51</sup> The initial configuration is a cell

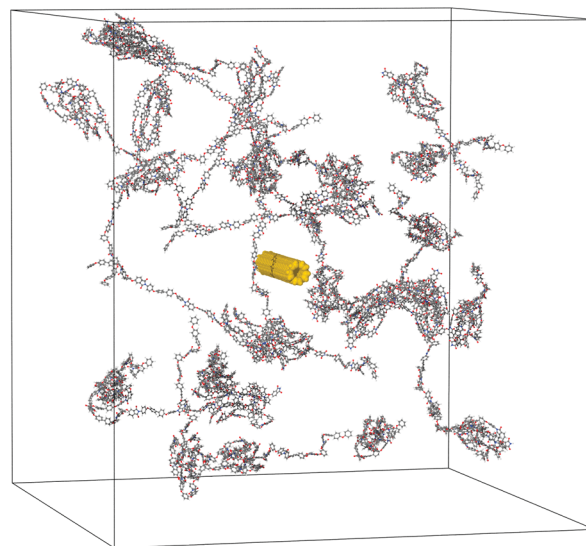


Fig. 2 Initial configuration of the R-BAPB – CNT composite.

with a rather big volume in which partly coiled polymer molecules practically do not overlap, and with a CNT embedded into the cell (Fig. 2). Polymer chains and CNT are able to move in the simulation cell and their mobility was not constrained. It was followed by a gradual compression with total duration of 20 ns. The maximum pressure value during the compression was 300 bar. After the system compression, annealing took place which comprised the gradual alteration of the system temperature from the maximum temperature of 600 K to the minimum temperature of 290 K with an increment of 50 K. The maximum annealing temperature exceeds the glass transition of R-BAPB and R-BAPS by over 100 K,<sup>15,18</sup> which is essential to the correct determination of thermophysical properties of PCMs that are known to depend on the maximum annealing temperature.<sup>99</sup> At each annealing stage, the system was simulated for 2 ns. The process of cooling down and heating up was repeated three times during the annealing.<sup>47</sup> After that the simulation was performed at the temperature of 600 K for 10 ns. Therefore, the total time of the preliminary equilibration amounted to 108 ns. Further simulations were conducted at the constant temperature (600 K) and pressure (1 atm).

Equilibration time in MD of polymer systems is often determined by the system density achieving the values close to experimental ones.<sup>47,81,87,100</sup> In the majority of papers on polymer simulation, the equilibration time does not exceed 100 ns.<sup>47,64,80,85–87,101–104</sup> In the studies devoted to the polyethylene and polypropylene crystallization process, the typical simulation duration lies within the range of several nanoseconds<sup>65–67,71,72</sup> to several tenths of nanoseconds.<sup>68–70,95</sup> This is due to quite a rapid progress of the crystallization in the simulated systems, which is considered to be related to the simple structure of macromolecules and the relatively small system size. Recently, papers have emerged with the simulation time of approx. 100 ns.<sup>98</sup>

The polymer system reaching the density value close to the experimental one does not yield an unambiguous estimate of the system achieving its equilibrium. Indeed, density fluctuations in

bulk PIs at the temperature of 600 K are defined by quite rapid relaxation processes with characteristic times of several nanoseconds,<sup>18</sup> and the simulation run of  $\sim 100$  ns considerably exceeds the relaxation times of the system density fluctuations. However, it was demonstrated that this equilibration time may be insufficient for PIs in a bulk to reach the equilibrium state because the displacement of the polyimide chains in the melt for the distance comparable to the chain size at the temperature exceeding the glass-transition temperature  $T_g$  lies in the microsecond time-scale.<sup>19,20</sup> It was shown that the density of PI sample does not depend on equilibration degree. At the same time, the mean values of the polymer gyration radius  $\langle R_g \rangle$  and the end-to-end distance  $\langle h \rangle$ , after the completion of about 100 ns equilibration procedure, may be significantly lower than the values calculated on a theoretical basis in the case of PI with polymerization degree  $n_p = 8$ .<sup>18-20</sup> The sizes of PI chains close to those calculated theoretically are sure to be reached after equilibrating the system for 1.0–1.5  $\mu$ s in the case of simulation without electrostatic interactions.<sup>19,20</sup> This timescale corresponds to the time of polymer chains displacement for the distance comparable to their size. Therefore, to obtain the polymer equilibrated configuration at the temperatures higher than  $T_g$ , microsecond-scale simulation is required.

The embedding of the filler interacting with the polymer into the matrix may slow down considerably the relaxation processes taking place in the sample. For this reason, when simulating PCMs, a legitimate question arises as to how the filler incorporation will affect the equilibration time. To answer this question, a 3  $\mu$ s simulation was performed for the composites, same as for the bulk PIs earlier.<sup>19,20,51</sup> Based on the simulation, the mean square displacement  $\langle \Delta r_{\text{com}}^2(t) \rangle$  was calculated for the centers of mass (COM) of polyimide chains in the PCM, and the nanotube COM:

$$\langle \Delta r_{\text{com}}^2(t) \rangle = \langle (\vec{r}(t_1) - \vec{r}(t_2))^2 \rangle \quad (1)$$

where  $\vec{r}(t_i)$  is the COM radius vector of the molecule at the time  $t_i$ . The times  $t_1$  and  $t_2$  are averaged out so that  $t = t_2 - t_1$ . The results obtained for the R-BAPB-based composites are shown as

an example in Fig. 3. The R-BAPS-based composites have yielded identical results.

The comparison of  $\langle \Delta r_{\text{com}}^2(t) \rangle$  for the PI chains in a bulk and in a composite (Fig. 3a) showed that the CNT embedding into the PI matrix hardly affects the mobility of the polymer chains. Therefore, the time necessary to reach the equilibrium configuration of the PCMs should coincide with the time required to equilibrate the bulk PIs. Indeed, polyimide chains in PCMs may reach the theoretically predicted size after the simulation for  $\sim 1.5$   $\mu$ s (Fig. 4). Notably, for R-BAPB composite, the PI chain size after a 3  $\mu$ s simulation turned out to be a little higher than the forecast value, whereas, in contrast, the chain size of the R-BAPS in PCM was a little lower than the value calculated theoretically. These discrepancies are likely to be caused by the altered chain shape in PCMs compared to the chain shape in the bulk PI samples. This phenomenon will be discussed in the following section.

As was demonstrated earlier<sup>20</sup> and as ensues from Fig. 3, electrostatic interactions lead to a loss of the mobility of the polymer chains and filler particles drastic. At fixed time, the mean square displacement of the polymer chains in the systems which were simulated taking electrostatic interactions into account is almost by two orders less than that for the neutral systems. The evaluation of the equilibrating time for these systems yields the value of about hundreds of microseconds, which is unattainable using available computing capacities. To overcome this problem, the two-step protocol proposed in our previous paper<sup>20</sup> was used to obtain PCM samples with electrostatic interactions. First, microsecond-scale equilibration of a sample with partial charges switched off was performed. Then 11 different polymer samples have been selected from the last microsecond of the 3  $\mu$ s equilibration run (every 100 ns during the 1  $\mu$ s run), *i.e.*, from the part of the MD trajectory where the system was proved to be in equilibrium. After that we switched the charges on and simulated these samples for 100 ns each.

The most widespread method used to assess the polymer matrix structure in PCMs is the computation of the pair distribution functions  $g(r)$  and various density distribution types of composite components.<sup>45,46,105–108</sup>

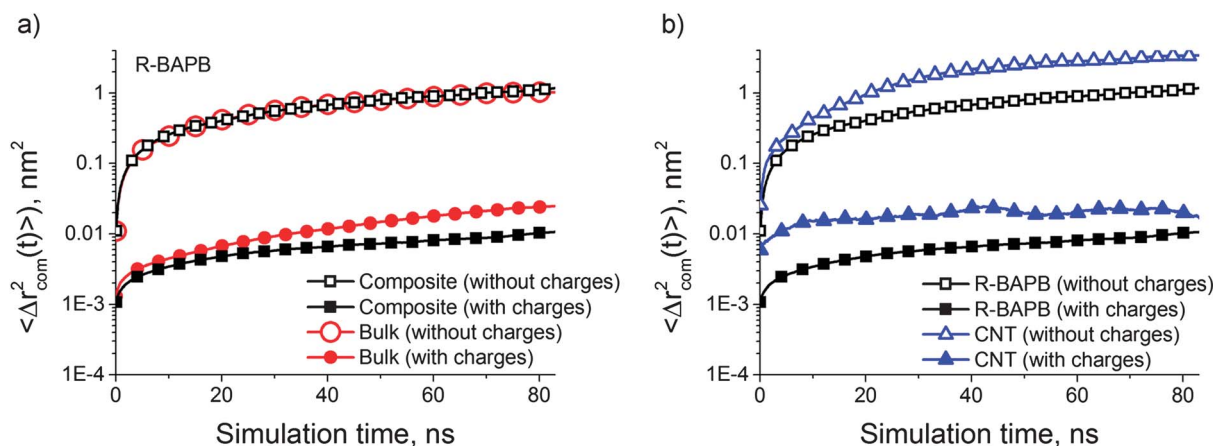


Fig. 3 Simulation time dependence of the mean square displacement (MSD) of the center of mass (COM) of the R-BAPB chains in a bulk or composite (a), and the COM MSD of R-BAPB chains and CNT in a composite (b), obtained during the simulation with and without electrostatic interactions.

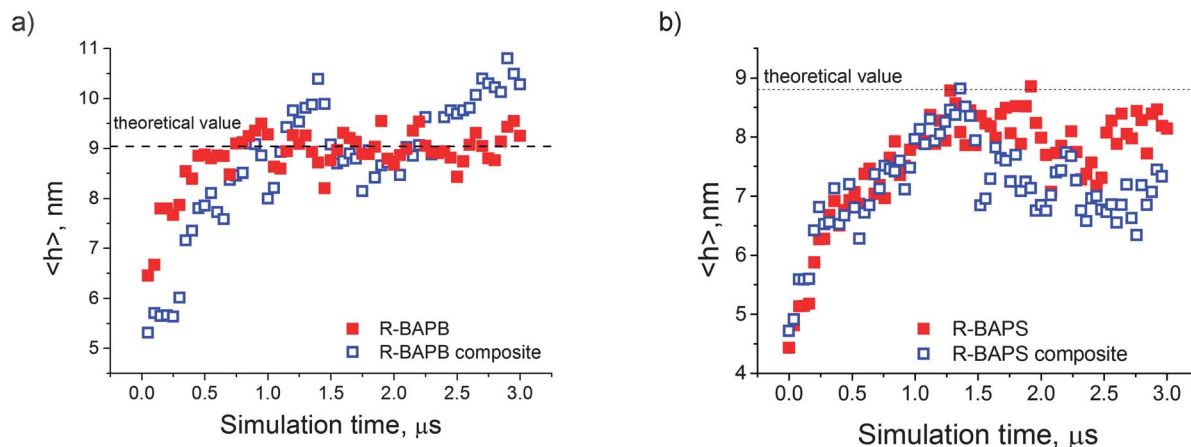


Fig. 4 Time dependence of the end-to-end distance  $\langle h \rangle$  of polymer chain during simulation of the bulk R-BAPB (a) and R-BAPS (b) polyimides and polyimide based PCMs.

To describe the polymer structure near the CNT, we have also calculated the pair distribution functions of polymer atoms in relation to the CNT atoms  $g_{\text{CNT-PI}}(r)$ , and the lateral distribution of the polymer density in relation to the CNT axis  $\rho(r)$ . To calculate these parameters, the eqn (2) and (3) have been used, respectively.

$$g_{\text{CNT-PI}}(r) = \frac{\langle \rho_{\text{PI}}(r) \rangle}{\langle \rho_{\text{PI}} \rangle_{\text{local}}} = \frac{1}{\langle \rho_{\text{PI}} \rangle_{\text{local}}} \frac{1}{N_{\text{CNT}}} \sum_{i \in \text{CNT}} \sum_{j \in \text{PI}} \frac{\delta(r_{ij} - r)}{4\pi r^2}. \quad (2)$$

Here  $\langle \rho_{\text{PI}}(r) \rangle$  is the average number density of the polymer atoms at the distance  $r$  to the CNT atoms, and  $\langle \rho_{\text{PI}} \rangle_{\text{local}}$  is the average number density of the PI in the system.  $N_{\text{CNT}}$  and  $N_{\text{PI}}$  are numbers of CNT and polyimide atoms, respectively,  $r_{ij}$  is the distance between the pair of CNT and PI atoms, and  $\delta$  is the Kronecker delta.

$$\rho(r) = \frac{m(r)}{4\pi h_{\text{CNT}} \Delta r (2r + \Delta r)}, \quad (3)$$

where  $m(r)$  is the mass of the polymer located in the cylindrical layer with the width  $\Delta r$  at the distance  $r$  from the CNT axis. The cylindrical layer height is determined by the nanotube length  $h_{\text{CNT}} \sim 4.7$  nm.

The shape of the polymer chains in a PCM is verified by the calculations of the mean radius of gyration of the chains  $\langle R_g \rangle$ , main components of the inertia tensor of the chains  $R_{g,x}$ ,  $R_{g,y}$  and  $R_{g,z}$ , as well as asphericity  $b$ , acylindricity  $c$  and relative anisotropy of the shape  $\kappa^2$ .<sup>109</sup>

The main components of the inertia tensor are determined by diagonalization of the tensor

$$G = \begin{bmatrix} R_{xx} & R_{xy} & R_{xz} \\ R_{yx} & R_{yy} & R_{yz} \\ R_{zx} & R_{zy} & R_{zz} \end{bmatrix}, \quad (4)$$

where components  $R_{\alpha\beta}$  ( $\alpha \in \{x,y,z\}$  and  $\beta \in \{x,y,z\}$ ) are calculated using the general equation:

$$R_{\alpha\beta} = \frac{\sum_i m_i (\alpha_i \beta_i - \alpha_C \beta_C)}{\sum_i m_i}. \quad (5)$$

Here,  $\alpha_i$  and  $\beta_i$  are coordinates of the  $i$ -th atom of the polymer chain, and  $\alpha_C$  and  $\beta_C$  are coordinates of the chain COM position. The diagonalization of the tensor  $G$  gives:

$$G_d = \begin{bmatrix} R_{g,x} & 0 & 0 \\ 0 & R_{g,y} & 0 \\ 0 & 0 & R_{g,z} \end{bmatrix}. \quad (6)$$

In this case, the relation  $R_{g,x} > R_{g,y} > R_{g,z}$  is maintained.

Parameters  $b$ ,  $c$  and  $\kappa^2$  describing the polymer shape are calculated using the values of the main components of chain inertia tensor:<sup>109</sup>

$$b = R_{g,x}^2 - 1/2(R_{g,z}^2 + R_{g,y}^2), \quad (7)$$

$$c = R_{g,y}^2 - R_{g,z}^2, \quad (8)$$

$$\kappa^2 = \frac{b^2 + (3/4)c^2}{R_g^4}. \quad (9)$$

## Results and discussions

The pair correlation functions  $g_{\text{CNT-PI}}(r)$  and lateral distributions of the polymer density in relation to CNT axis  $\rho(r)$  for R-BAPB and R-BAPS-based PCMs simulated with partial charges are shown in Fig. 5. Similar polymer-nanotube distribution functions were obtained in other nanocomposite simulation studies as well.<sup>105,106,108</sup>

Values of distance  $0 < r < 0.2$  where  $g_{\text{CNT-PI}}(r) = 0$  (Fig. 5a) correspond to the area which polyimide atoms cannot occupy due to their own atomic size. The rise of  $g_{\text{CNT-PI}}(r)$  within the range  $0.2 < r < 1.0$  to reach the values close to 1 takes place by accounting for the polyimide atoms forming the subsurface matrix layer. The small peak at  $r \sim 1$  nm corresponds to the atoms located in the subsurface layer of the polymer matrix.

With the values of  $r$  lower than the CNT diameter ( $d_{\text{CNT}} \sim 0.7$  nm), the pair distribution function takes into account the matrix atoms which are found near the nanotube external surface only. With  $r > d_{\text{CNT}}$  the matrix atoms which are located on the strictly opposite side of the CNT in relation to its

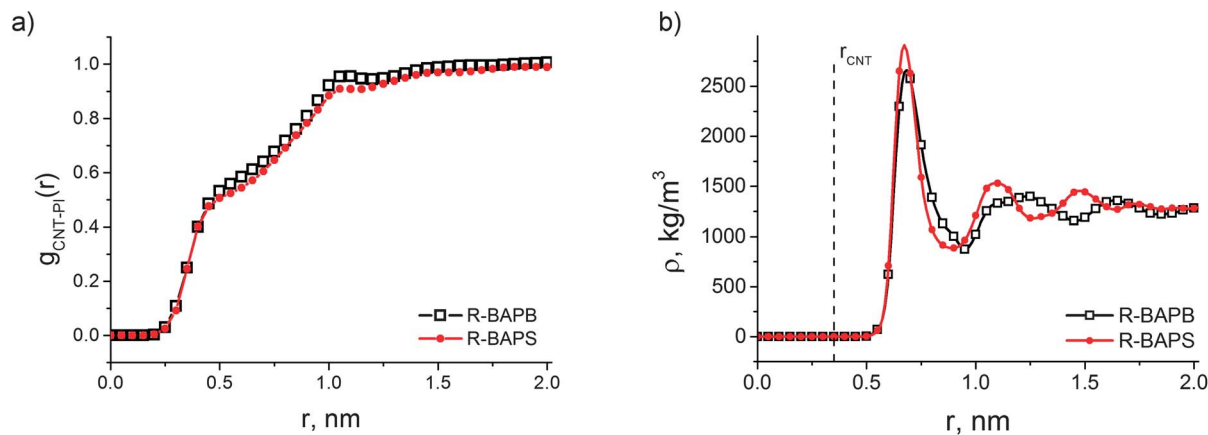


Fig. 5 Pair distribution functions  $g_{\text{CNT-PI}}(r)$  of the polymer atoms in the composites simulated with full electrostatics in relation to the CNT atoms (a), and the distribution of the polymer density  $\rho(r)$  relative to the CNT axis (b) for R-BAPB and R-BAPS-based PCMs. Dashed line corresponds to the CNT radius  $r_{\text{CNT}}$ . The inset in (b) shows a zoomed-in area selected by the rectangle.

specific atom come into account in the pair correlation function  $g_{\text{CNT-PI}}(r)$ . The kink of the curve at  $r = 0.5\text{--}0.7$  nm, which is usually not considered,<sup>105,106,108</sup> is likely to be associated with atoms located at a distance exceeding the CNT diameter from the specific carbon atom of the nanotube.

The dependence obtained for the polymer density distribution in relation to the CNT axis (Fig. 5b) is qualitatively similar for the R-BAPB and R-BAPS-based PCMs. Polymer in nanocomposites forms “shells” (this corresponds to some local structuring of PI atoms) around the nanoparticle with the polymer density exceeding the average polymer density in the system. Near the CNT surface (at a distance of  $\sim 0.6$  to  $0.8$  nm from its axis), there is an area with the polymer density considerably exceeding the average system density. This area corresponds to the polymer matrix atoms which are closest to the CNT surface and form the subsurface layer where flat fragments of PI polymer chain are oriented along the CNT axis as will be shown below. The distance dependence of PI density obtained in the present study coincides qualitatively with the nanocomposites simulation results described above.<sup>45,110</sup>

The difference in positions of density peaks that is observed for R-BAPB and R-BAPS (Fig. 5b) is due to the presence of the highly charged sulfonic group in the R-BAPS monomer unit. Higher partial charges in R-BAPS lead to rather strong dipole-dipole interactions and to additional local structuring, as shown in our previous study.<sup>18</sup> Thus, the presence of the sulphone group in the diamine fragment results in a denser packing of R-BAPS in comparison with R-BAPB, which, in turn, leads to the lower distance between peaks.

The pair distribution functions  $g_{\text{CNT-PI}}(r)$  and the polymer density distribution in the composite  $\rho(r)$  are determined by the atomic composition of the polymer matrix and do not account for its chemical structure. R-BAPB and R-BAPS have a rather similar atomic composition, which is why for PCMs based on them,  $g_{\text{CNT-PI}}(r)$  and  $\rho(r)$  are quite similar as well and do not provide sufficient information on the polymer matrix microstructure. Therefore, the pair distribution functions in the PCM which are generally used to describe the material

structure,<sup>45,46,105–108</sup> do not clarify the interrelation between the composite microscopic structure and the matrix-building polymer chemical structure. Thus, some additional characterization of the subsurface layer microstructure is needed.

In order to describe further the subsurface layer microstructure of the polymer matrix in PCMs, we have calculated the distribution of the angle  $\theta$  between the CNT axis and vectors defining the position of flat fragments of PI monomer units and order parameter  $S(r)$  for these vectors. The fragments of the PI monomer units for which the orientation-related parameters were calculated have been chosen so that their geometrical configuration would be close to a flat one, which enables us to reduce the impact of the valence angle value fluctuation on the distributions obtained. For R-BAPB, phenylphthalimide and diphenyl fragments have been chosen for this purpose. In Fig. 1, these fragments are marked as PPI and DP, respectively. For R-BAPS, to calculate  $S(r)$  and  $\theta(r)$ , phenylphthalimide and diphenylsulfone fragments have been chosen which are marked as PPI and DPS in Fig. 1. The diphenylsulfone fragment DPS is not flat due to the presence of sulfone group. Nevertheless, the order parameter  $S(r)$  and angle distribution  $\theta(r)$  calculation for this fragment will make it possible to investigate the influence of the sulfone group presence on the orientation of the polymer chain fragments along the CNT.

The order parameter  $S(r)$  was calculated using the following equation:

$$S(r) = 3/2 \langle \cos^2 \theta(r) \rangle - 1/2 \quad (10)$$

where  $\langle \cos^2 \theta(r) \rangle$  is the mean square of the angle cosine between the CNT axis and the vector of the PI monomer unit fragment arranged at a distance  $r$  from the CNT axis.

As far as the CNT has a highly curved surface, it is interesting to explore the flat fragments distribution in the azimuthal direction relative to the nanotube axis. The azimuthal dependence of the order parameter  $S(\varphi, r)$ , where  $\varphi$  is an azimuthal angle, was calculated for the PPI fragments of R-BAPB and R-BAPS polyimides which are located in the most dense PI

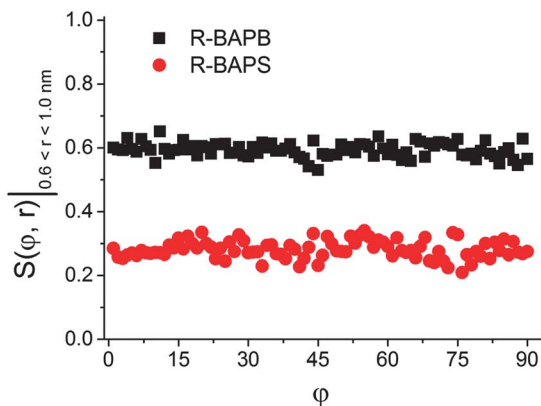


Fig. 6 Azimuthal dependence of the order parameters  $S(\phi, r)$  of the PPI flat fragments of R-BAPB and R-BAPS polyimides calculated in the region  $0.6 < r < 1.0$  nm for PCM systems simulated with electrostatic interactions.

region close to the CNT surface ( $0.6 < r < 1.0$  nm as follows from Fig. 5b). The results obtained are shown in Fig. 6. As seen from this figure, there is no significant azimuthal dependence of the order parameter of PPI fragments for both PIs, *i.e.* the azimuthal distribution of polymer for the chosen CNT diameter is rather uniform.

The order parameter  $S(r)$  and distributions of the orientation angles of PPI fragments in relation to the CNT axis  $\theta(r)$  calculated for the composites based on R-BAPB and R-BAPS simulated with electrostatic interactions are shown in the Fig. 7. The averaging of the calculated characteristics was performed within the time interval of 40 ns with instantaneous configurations taken every 20 ps. Therefore, each  $\theta(r)$  distribution shown below is obtained by averaging 2000 configurations per each system studied.

The first peak in the order parameter dependence  $S(r)$  (Fig. 7a and b) corresponds to the subsurface layer of PIs. The formation of this layer at  $T = 600$  K was observed in all simulated PCMs. The position of the subsurface layer correlates with the first peak of the polymer density distribution functions (Fig. 5b).

The order parameters are very similar for the systems calculated with and without electrostatic interactions in the region of the subsurface layer ( $r < 1.2$  nm). Rather high fluctuations are observed for  $S(r)$  of the systems with electrostatic interactions. However,  $S(r)$  dependences are qualitatively similar in both cases. For the R-BAPS-based PCMs the rapid decrease of the order parameter to zero is observed, whereas only slow decrease is observed for the R-BAPB-based PCMs. Such behavior allows us to suppose that some orientational ordering is observed in PCMs based on the R-BAPB.

The analysis of the orientation angle distributions  $\theta(r)$  (Fig. 7c and d) shows that the polymer is found primarily along the CNT in the subsurface layer. For the first layer positioned at the distance of 0.8 nm from the CNT axis and about 0.3–0.4 nm wide, the angle distribution peak is observed at  $\theta \sim 10$ – $20^\circ$ . The analysis of the microstructure of the polymer located farther away from the CNT is impeded, because  $\theta(r)$  distribution is fragmented due to the strong local structuring observed for the

systems simulated with electrostatic interactions. Such local structuring results from the strong dipole–dipole interactions in these systems and leads to the formation of polymer shells with increased density seen on the Fig. 5b.

Unfortunately, the structural analysis of considered PCMs simulated with full electrostatics for  $\theta(r)$  distributions is rather complicated due to the observable high fluctuations. The strong deceleration of polymer chains movement in the matrix,<sup>20</sup> (Fig. 3) leads to the “freezing” of the polymer matrix microstructure in the systems with electrostatic interactions accounted for. This impedes the polymer microstructure statistical analysis considerably since it requires simulation of much larger systems, and a longer and more resource-intensive simulation procedure that is impossible due to computational resources limitation.

Taking into account that the partial charges of the CNT atoms slightly differ from zero only on the CNT ends (more than 80% of CNT atoms have zero charges, see ESI†), one can conclude that the electrostatic interactions should not influence sufficiently the orientation ordering of PI chains in the PCMs close to the CNT surface, which is probably governed mostly by excluded volume interactions. Consequently, it is more convenient to investigate the PI chains orientation structuring by studying PCMs without electrostatic interactions. Indeed, the comparison of orientation angle distribution  $\theta(r)$  of PPI fragments for the systems with and without electrostatic interactions obtained after the same simulation time (Fig. 7e–f) results in the similar conclusions about the orientation structuring of PI chains near the CNT surface. Thus, all the results presented below correspond to the systems without electrostatic interactions to perform more detailed analysis of the CNT-induced local structuring of PI chains.

To study the influence of the PCM equilibration degree on the polymer matrix microstructure, calculations were conducted for several samples taken at different equilibration times: from 0.5  $\mu$ s to 3.0  $\mu$ s with an increment of 500 ns.

It was established that the equilibrated microstructure of the polymer matrix in R-BAPS-based composites takes quite long to form. Changes in the angle distribution between the CNT axis and PPI flat fragments of polymer units for these PCMs take place during equilibration stage of  $\sim 1.5$   $\mu$ s, which ensues from the alteration of the order parameters for the fragments of the R-BAPS monomer units in composites based on this polymer (Fig. 8b). The polymer microstructure of R-BAPB-based composites takes final form after the 500 ns equilibration already.

Typical distributions of the angle  $\theta(r)$  depending on the distance  $r$  between the vector corresponding to the PPI fragments of R-BAPB and R-BAPS monomer units, and the CNT axis obtained after equilibration stage are shown in Fig. 7e and f, respectively.

For R-BAPS, the angle  $\theta$  distribution does not essentially depend on the distance to the CNT axis. The values of the angle  $\theta$  in this case are distributed over a wide interval with a peak close to  $90^\circ$ , which is a mean value for the range of possible values of the angle  $\theta$  varying from  $0^\circ$  to  $180^\circ$ . For this polymer,

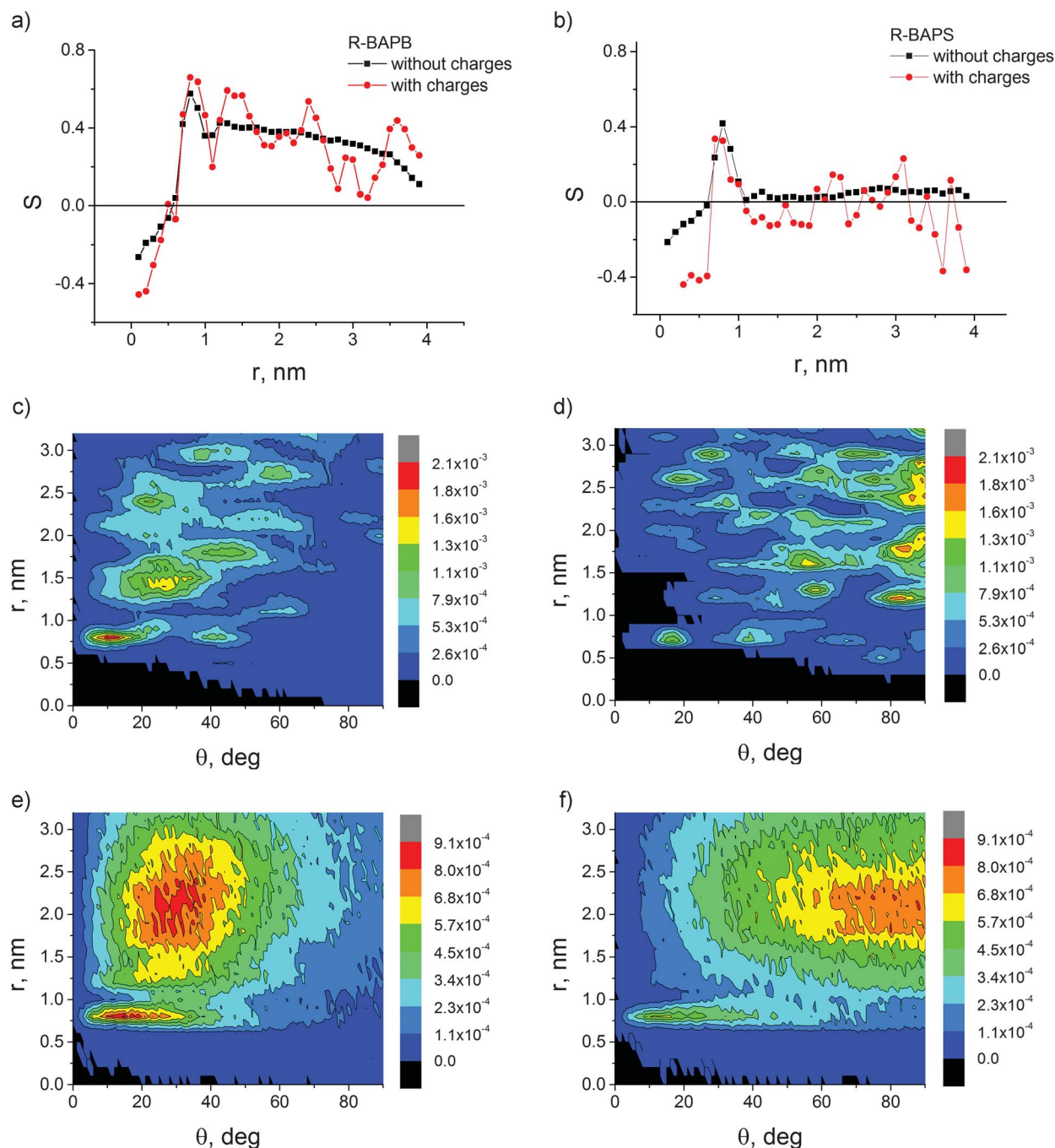


Fig. 7 Order parameters for the same fragments of the monomer units of R-BAPB (a) and R-BAPS (b) calculated after the 2.0  $\mu\text{s}$  simulation time with and without electrostatic interactions. Distribution of the angle  $\theta(r)$  between the CNT axis and the vector corresponding to the PPI flat fragments of the monomer units of R-BAPB (c and e) and R-BAPS (d and f) in composites calculated after 2.0  $\mu\text{s}$  simulation with (c and e) and without (d and f) electrostatic interactions.

certain ordering of the chains is observed mainly near the CNT surface only, and is not found away from it.

At the same time, in the case of R-BAPB, the polymer forms structure with several “layers”. Each layer shows its own peak at  $\theta(r)$  shifted towards larger values. We can say that R-BAPB-based nanocomposites demonstrate a “memory effect”, that is the orientation of the monomer units far away from the filler surface depends on how the polymer chains are oriented closer to the CNT surface.

The conclusions drawn are verified by the analysis of the dependence of the calculated order parameter  $S(r)$  (eqn (10)) on the distance between the flat fragment of the PI monomer unit and the CNT axis in the composite (Fig. 8).

The first peak observed for the order parameters of the both types of PCMs corresponds to the subsurface polymer layer near the filler particle as was mentioned before. The subsequent slow decrease of the order parameter for the R-BAPB-based composites confirms the “memory effect” present in these

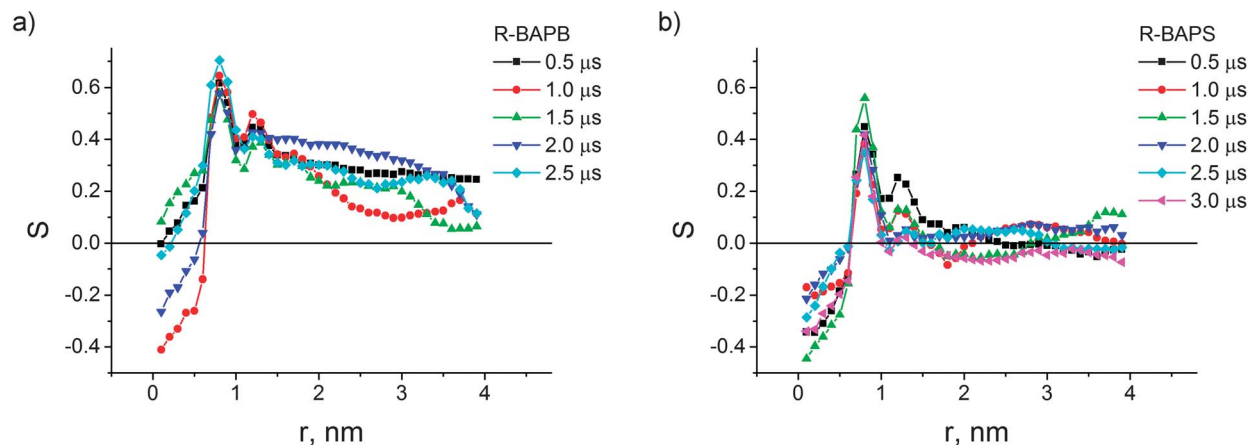


Fig. 8 Order parameter  $S(r)$  for flat PPI fragments of R-BAPB (a) and R-BAPS (b) in composites calculated for the samples produced after different simulation time.

PCMs. The quite high second peak in  $S(r)$  dependence for the R-BAPB-based composites with the value  $r \sim 1.2$  nm indicates the building-up of the polymer “layered” structure near the CNT surface. The fast decrease of the order parameter to zero in the R-BAPS-based composites shows that the long-range order is not present beyond the subsurface layer in these PCMs.

In our opinion, the formation of such a structure may constitute the initial stage of the PI matrix crystallization where the CNT acts as the nucleation center. The present study is the first report on the nucleation effect observed for PI-based PCM using MD simulations.

It should be noted that the dependence of the order parameter on the equilibration time is also indicative of a considerable influence of the polymer equilibration degree on the interface area structure in the PCM.

The comparison of the angle distribution  $\theta(r)$  between the CNT axis and different fragments of PI monomer units (Fig. 9) shows that in the R-BAPB-based composites, the consequent PPI and DP flat fragments are ordered in the same way. Both fragments orient along the CNT in the matrix subsurface layer and form the partly ordered structure with an increased distance from the CNT surface. Order parameters  $S(r)$  for both fragments of R-BAPB polymer units are almost the same.

In the case of R-BAPS, ordering of the monomer chain fragments along the CNT surface is observed only for the PPI flat fragment, whereas the DPS fragment displays no significant ordering even near the CNT surface. This also ensues from the angle orientation distribution of the DPS fragment along the CNT in R-BAPS-based composites, and from the order parameter.

The consequent flat fragments are aligned both near the CNT surface and away from it. Embedding of the sulfone group leads to the disordering of the DPS fragment containing this group accompanied by the drop in the order parameter for the flat PPI fragment.

Since the R-BAPB chain contains several flat fragments following each other, the CNT in the PCM is likely to act as an object setting the orientation not only of separate fragments of the polymer chain but of the entire chain as well. Indeed, the

visual check of the instantaneous configurations showed that the R-BAPB-based composites have oblong-shaped PI chains (Fig. 10), with a separate PI chain interacting generally with several periodical images of the CNT. The study of the influence of PI chains interactions with periodic images of CNT on the matrix microstructure requires additional simulations of larger systems, and is the subject of our ongoing work.

The characteristics of polymer chains size and shape calculated for the systems without electrostatic interactions are given in Table 1 (for the systems with electrostatic interactions similar results were obtained).

In the R-BAPB-based composites, the polymer chain gyration radius rises by approx. 10% compared to the chain size in the bulk sample, and the PI chain shape changes as well. Increased values of the shape relative anisotropy  $\kappa^2$ , shape factor  $R_{g,x}/R_{g,z}$  and asphericity  $b$  accompanied by a drop in the chain acylindricity  $c$  testifies to the fact that the R-BAPB chains in a PCM with a CNT as filler are elongated. As ensues from the orientation angle distribution of the flat fragments of the R-BAPB monomer units in relation to the CNT axis, the draw direction is set by the nanotube position.

At the same time, the R-BAPS-based composite demonstrates an inverse effect. The gyration radius, relative shape anisotropy and shape factor of R-BAPS chains in the PCM are even somewhat lower than these in bulk. Compared to the bulk PI, R-BAPS in composite has a lower value of the chain asphericity and a higher acylindricity value. Therefore, R-BAPS chains in the PCM with a CNT get more compact sphere-like structure. This effect is likely to be due to the fact that, as well as enhancing the flexibility of PI chain, the embedding of the sulfone group influences their geometry increasing their “bending degree”. Consequently, the coiled molecule conformations become more efficient.

To study further the impact of the chemical modification of the PI repeating unit by the sulfone group on the size and shape of polyimide chains in a PCM, we have performed an additional simulation of the bulk polyimide EXTEM™ (ref. 111) with a chain polymerization degree of  $n = 9$  and corresponding PCMs. Currently, this PI produced by Sabic Innovative Plastics is one of

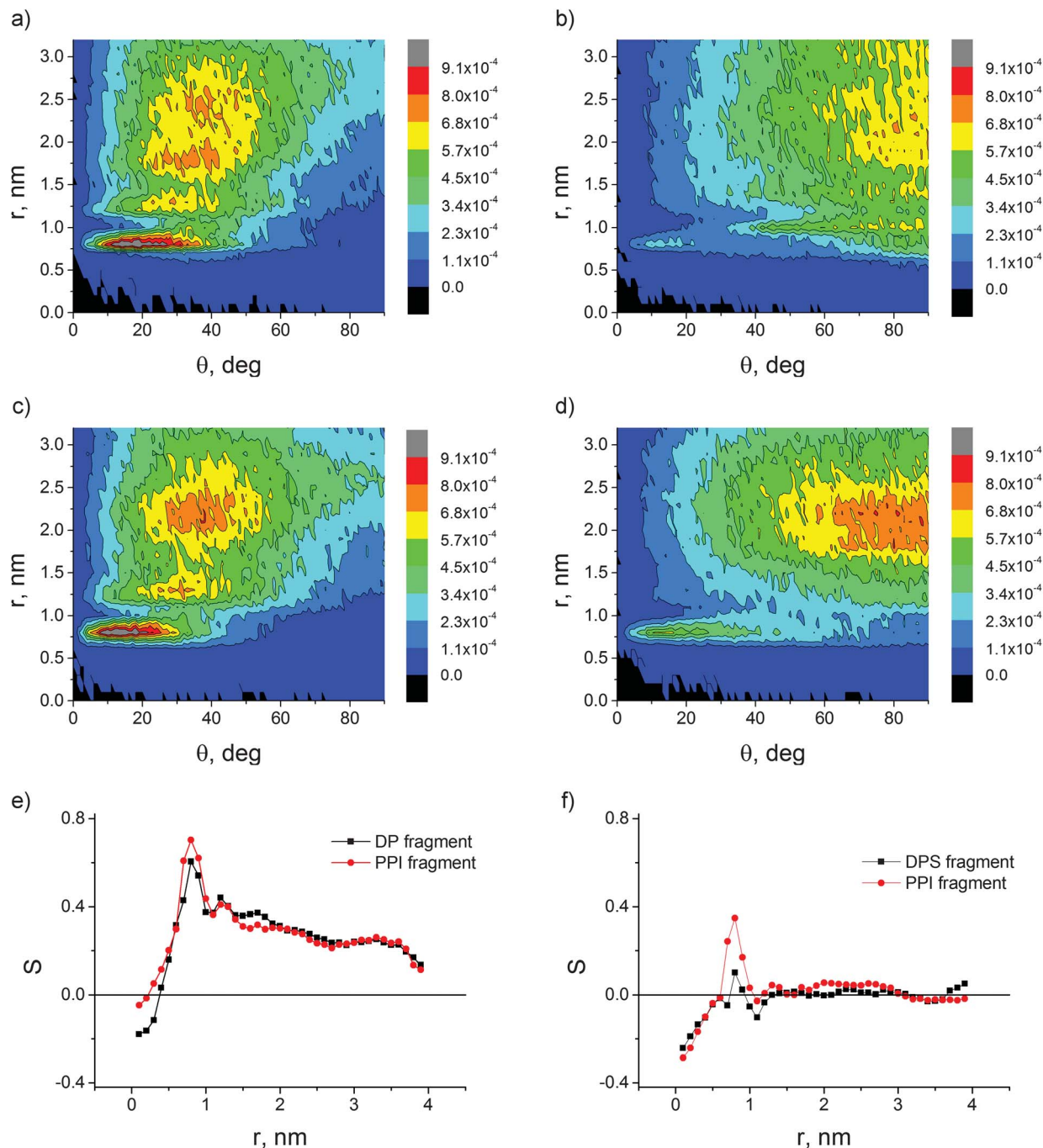


Fig. 9 Distribution of the angle  $\theta$  between the CNT axis and the vector corresponding to the DP (a), DPS (b) and PPI (c and d) fragments of the monomer units of R-BAPB (a and c) and R-BAPS (b and d) in the composites calculated after the 2.5  $\mu\text{s}$  simulation. Order parameters for polymer R-BAPB (e) and R-BAPS (f) calculated with the same simulation time for different fragments of PI monomer units.

the most promising polyimides for practical use due to its high glass-transition temperature. The structural formula of EXTEM<sup>TM</sup> is given in Fig. 1 (bottom). The monomer unit of this PI, similar to the R-BAPS monomer unit, contains a DPS fragment. The complete simulation procedure is computationally demanding; a shorter 1  $\mu\text{s}$  simulation was performed for the EXTEM<sup>TM</sup>-based systems after the annealing. For EXTEM<sup>TM</sup> in a bulk and in a PCM, the chain size and shape characteristics were calculated. The results are also presented in Table 1.

Both EXTEM<sup>TM</sup> and R-BAPS are characterized by a certain drop in the chain gyration radius in the PCM, compared to that in the bulk, though the chain shape, same as in the R-BAPS-based composites, does not undergo considerable changes. This is supported by the similar values of the shape factor and relative anisotropy of the EXTEM<sup>TM</sup> chain shape in the PCM and in bulk.

Therefore, one might assume that the presence of sulfone group in the polyimide monomer unit impacting the chain flexibility and spatial configuration prevents the chains from

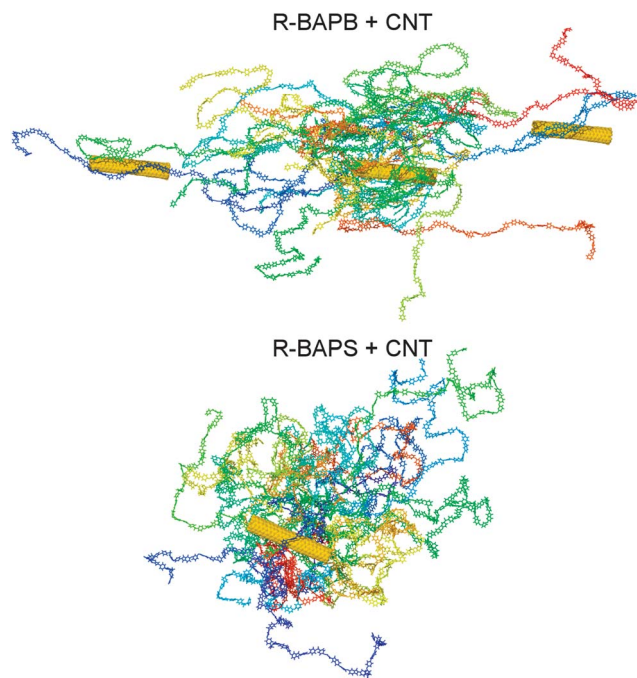


Fig. 10 Typical snapshots of R-BAPB (top) and R-BAPS (bottom) composites obtained after the 2.5  $\mu$ s simulation. Each molecule is highlighted in its own color. For the R-BAPB-based composite, two periodic images of the primary CNT are shown.

spreading out along the CNT in the PCMs, and forming the ordered structure in the PI matrix.

The structural difference between R-BAPS and R-BAPB must be attributed to the fact that the chains of the latter are stiffer and can form structures maintaining the order at a greater distance from the CNT surface due to the mutual orientation of the macromolecule flat fragments. The similar effect was observed recently in the case of nanoconfined films of glass-forming polymers. In these films some local ordering was observed only in the case of polymer with most rigid backbone.<sup>112</sup> The results obtained for R-BAPB composites qualitatively correlate with the experimental data on crystallization of this polyimide in PCMs where the filler particle (carbon tube or carbon fiber) acted as the nucleation center.<sup>21,23–25</sup>

The formation of a partly ordered structure near the CNT surface in the R-BAPB composite matrix observed in simulation may be regarded as the initial part of the polymer matrix crystallization process. The instability of the polymer structure

formed near the CNT may be attributed to the fact that the simulation temperature exceeds the R-BAPB melting point.<sup>15</sup> The formation of ordered structures at lower temperatures requires more simulation time and essentially larger computing resources.

The driving force behind the formation of structures with a memory effect is likely to be the interaction of aromatic fragments in PI chains with the CNT surface and with each other, which results in ordering the chain position in the polymer matrix and forming the partly ordered microstructure. CNT position sets the spatial direction along which PI chain flat fragments are oriented, which may facilitate the formation of stable ordered structures. At the same time, the simulation results demonstrate that electrostatic interactions play no significant role in the formation of such structures in PCMs, but lead to local ordering in PI matrix due to rather strong dipole–dipole interactions.

## Conclusions

This paper presents an extensive molecular dynamics simulation of polymer composite materials (PCM) based on two types of heat-resistant polyimides (PI) with a carbon nanotube (CNT) as filler.

Similar to the bulk PI simulations,<sup>18–20,51</sup> it has been discovered that equilibrium chain size values are reached only after equilibration of the systems containing PIs with polymerization degree  $n_p = 8$  without electrostatic interactions for  $\sim 1.5 \mu$ s at the temperature of 600 K. The investigation of the microstructure of PCMs with different equilibration times showed that the microstructure of the simulated systems depends on the polymer equilibration degree.

The nanocomposite simulations with and without electrostatic interactions demonstrated that the amount of electrostatic interactions does not have a considerable impact on the polymer matrix microstructural organization (initial crystallization stage) near the filler nanoparticle surface. In this case it is more reasonable to analyze the orientation ordering of polymer chains in the matrix using the simulation without electrostatic interactions (with zero partial charges) since the partial charges cause rather strong local ordering in the PI matrix, as well as a rather sharp drop in the mobility of polymer chains provoking the microstructure “freezing” and complicating its statistical analysis. At the same time, the electrostatic interactions are of crucial importance for the determination of the macroscopic thermophysical properties of polymers, such as

Table 1 Gyration radius  $R_g$ , components of the inertia tensor  $R_{g,x}$ ,  $R_{g,y}$  and  $R_{g,z}$ , shape factor  $R_{g,x}/R_{g,z}$ , asphericity  $b$ , acylindricity  $c$  and relative shape anisotropy  $\kappa^2$  of R-BAPB and R-BAPS chains in composites and in a bulk sample calculated without electrostatic interactions (averaging was made over last 500 ns of 3  $\mu$ s simulations)

	$R_g$	$R_{g,z}$	$R_{g,y}$	$R_{g,x}$	$R_{g,x}/R_{g,z}$	Asphericity $b$	Acylindricity $c$	Shape anisotropy $\kappa^2$
R-BAPB bulk	$3.64 \pm 0.07$	$1.59 \pm 0.06$	$1.92 \pm 0.07$	$2.65 \pm 0.04$	$1.67 \pm 0.07$	$3.9 \pm 0.3$	$1.2 \pm 0.2$	$0.09 \pm 0.02$
R-BAPB composite	$4.03 \pm 0.05$	$1.51 \pm 0.04$	$1.74 \pm 0.06$	$3.30 \pm 0.06$	$2.19 \pm 0.05$	$8.3 \pm 0.4$	$0.7 \pm 0.2$	$0.26 \pm 0.02$
R-BAPS bulk	$3.15 \pm 0.06$	$1.53 \pm 0.04$	$1.82 \pm 0.08$	$2.08 \pm 0.06$	$1.36 \pm 0.06$	$1.5 \pm 0.4$	$1.0 \pm 0.2$	$0.03 \pm 0.01$
R-BAPS composite	$2.94 \pm 0.04$	$1.52 \pm 0.04$	$1.62 \pm 0.04$	$1.93 \pm 0.06$	$1.27 \pm 0.06$	$1.27 \pm 0.06$	$0.3 \pm 0.1$	$0.02 \pm 0.01$
EXTEM™ bulk	$3.06 \pm 0.02$	$1.43 \pm 0.03$	$1.87 \pm 0.03$	$1.96 \pm 0.02$	$1.37 \pm 0.04$	$1.1 \pm 0.1$	$1.5 \pm 0.1$	$0.03 \pm 0.01$
EXTEM™ composite	$2.97 \pm 0.04$	$1.49 \pm 0.03$	$1.59 \pm 0.02$	$2.01 \pm 0.04$	$1.35 \pm 0.02$	$1.7 \pm 0.1$	$0.3 \pm 0.1$	$0.04 \pm 0.01$

the glass-transition temperature and the volumetric thermal expansion coefficient.<sup>20</sup>

For all PCMs, at the temperature of 600 K the polymer builds up the subsurface layer near the CNT surface where the polymer chains are oriented mainly along the filler. This layer is ~1 nm thick.

PCMs with a matrix based on the R-BAPB which is crystallizable and has stiffer chains compared to the R-BAPS, show a “memory effect” consisting of maintaining the orientation direction of the PI chain flat fragments as they move away from the filler surface. It results in forming an ordered microstructure which is likely to be regarded as the initial stage of the polymer crystallization in the composite that is observed experimentally.<sup>21,23–25</sup>

The present simulation also makes assertions that the incorporation of groups enhancing the polymer chain flexibility into the PI repeating unit leads to a decrease in the polymer order degree in the matrix at a remote distance from the nanofiller surface.

R-BAPB-based composites reveal the PI chains aligning along the direction set by the spatial position of the CNT, which is accompanied by a considerable alteration of the polymer chain size compared to that in the polyimide in a bulk. At the same time, R-BAPS-based composites feature some chain size reduction compared to the bulk PI. A similar effect has been observed for the PCMs based on polyimide EXTEM™ also containing a sulfone group. Therefore, the influence was demonstrated of the incorporation of a hinge sulfone group into the PI repeating unit on the properties of the polymer matrix near the filler in a PCM.

Issues to be addressed in forthcoming research include the impact of different types of nanofiller geometry as well as other types of hinge groups (e.g. ether or methylene groups) incorporated into the PI chemical structure, on the microstructure of the polymer matrix near the filler surface.

## Acknowledgements

This study was carried out under the financial support of the Russian Ministry of Education and Science (State Agreements no. 8023 and no. 8645, State Contract no. 16.523.12.3001 (Joint Russia-EC “COMPANOCOMP” project under the FP7 framework)) and Russian Foundation for Basic Research (Projects 11-03-00944-a and 13-03-00547-a). The simulations were carried out with the use of the computational resources of the Institute of Macromolecular Compounds, Russian Academy of Sciences, and the Chebyshev and Lomonosov supercomputers at Moscow State University. Authors are thankful to Prof. A. Khokhlov for fruitful discussions.

## Notes and references

- 1 A. Baker, S. Dutton and D. Kelly, *Composite materials for aircraft structures*, American Institute of Aeronautics and Astronautics, Inc, Reston, Virginia, 2nd edn, 2004.
- 2 A. P. Mouritz and A. G. Gibson, *Fire properties of polymer Composite materials*, Springer, Dordrecht, 2006.
- 3 D. Gay, S. V. Hoa and S. W. Tsai, *Composite materials. Design and application*, CRC Press, London, 2003.
- 4 *Multifunctional Polymer Nanocomposites*, ed. J. Leng and L. A. Kin-tak, CRC Press, London, 2010.
- 5 E. D. Laird and C. Y. Li, *Macromolecules*, 2013, **46**, 2877.
- 6 S. S. Ray and M. Okamoto, *Prog. Polym. Sci.*, 2003, **28**, 1539.
- 7 M. I. Bessonov, M. M. Kotton, V. V. Kudryavtsev and L. A. Lajus, *Polyimides – thermally stable polymers*, Consultants Bureau, New York, 1987.
- 8 *Polyimides: Fundamentals and Applications*, ed. M. K. Ghosh and K. L. Mittal, Marcel Dekker Inc., New York, 1996.
- 9 H. Ohya, V. V. Kudryavtsev and S. I. Semenova, *Polyimide Membranes-Applications, Fabrication and Properties*, co-published by Kodansha Ltd. and Gordon and Breach Science Publishers S.A., Tokyo and Amsterdam, 1996.
- 10 M. J. M. Abadie and A. L. Rusanov, *Practical Guide to Polyimides*, Smithers Rapra Technology Limited, Shawbury, 2007.
- 11 Q.-Y. Tang, Y.-C. Chan, N.-B. Wong and R. Cheung, *Polym. Int.*, 2010, **59**, 1240.
- 12 C. Park, Z. Ounaies, K. A. Watson, R. E. Crooks, J. Smith Jr, S. E. Lowther, J. W. Connell, E. J. Siochi, J. S. Harrison and T. L. St. Clair, *Chem. Phys. Lett.*, 2002, **364**, 303.
- 13 S. M. Yuen, C.-C. M. Ma, Y.-Y. Lin and H.-C. Kuan, *Compos. Sci. Technol.*, 2007, **67**, 2564.
- 14 G. He, J. Zhou, K. Tan and H. Li, *Compos. Sci. Technol.*, 2011, **71**, 1914.
- 15 V. E. Yudin and V. M. Svetlichnyi, *Russ. J. Gen. Chem.*, 2010, **80**, 2157.
- 16 H. Xu, H. Yang, L. Tao, J. Liu, L. Fan and S. Yang, *High Perform. Polym.*, 2010, **22**, 581.
- 17 V. E. Yudin, G. M. Divoux, J. U. Otaigbe and V. M. Svetlichnyi, *Polymer*, 2005, **46**, 10866.
- 18 S. V. Lyulin, S. V. Larin, A. A. Gurtovenko, N. V. Lukasheva, V. E. Yudin, V. M. Svetlichnyj and A. V. Lyulin, *Polym. Sci., Ser. A*, 2012, **54**, 631.
- 19 V. M. Nazarychev, S. V. Larin, N. V. Lukasheva, A. D. Glova and S. V. Lyulin, *Polym. Sci., Ser. A*, 2013, **55**, 570.
- 20 S. V. Lyulin, A. A. Gurtovenko, S. V. Larin, V. M. Nazarychev and A. V. Lyulin, *Macromolecules*, 2013, **46**, 6357.
- 21 V. E. Yudin, V. M. Svetlichnyj, A. N. Shumakov, R. Schechter, H. Harel and G. Marom, *Composites, Part A*, 2008, **39**, 85.
- 22 T. Kurose, V. E. Yudin, J. U. Otaigbe and V. M. Svetlichnyj, *Polymer*, 2007, **48**, 7130.
- 23 V. E. Yudin, V. M. Svetlichnyi, A. N. Shumakov, D. G. Letenko, A. Y. Feldman and G. Marom, *Macromol. Rapid Commun.*, 2005, **26**, 885.
- 24 V. E. Yudin, A. Y. Feldman, V. M. Svetlichnyi, A. N. Shumakov and G. Marom, *Compos. Sci. Technol.*, 2007, **67**, 789.
- 25 V. E. Yudin, V. M. Svetlichnyi, G. N. Gubanova, A. L. Didenko, T. E. Sukhanova, V. V. Kudryavtsev, S. Ratner and G. Marom, *J. Appl. Polym. Sci.*, 2002, **83**, 2873.
- 26 D. Bikiaris, *Materials*, 2010, **3**, 2884.
- 27 Z. Pu, H. Tang, X. Huang, J. Yang, Y. Zhan, R. Zhao and X. Liu, *Colloids Surf., A*, 2012, **415**, 125.

- 28 J. Zhong, H. Tang, Y. Chen and X. Liu, *J. Mater. Sci.: Mater. Electron.*, 2010, **21**, 1244.
- 29 *Hybrid Nanocomposites for Nanotechnology: Electronic, Optical, Magnetic and Biomedical Applications*, ed. L. Merhari, Springer, 2009.
- 30 *Recent Advances in Elastomeric Nanocomposites (Advanced Structured Materials)*, ed. V. Mittal, J. K. Kim and K. Pal, Springer, 2011.
- 31 *Polymer nanocomposites*, ed. Y.-W. Mai and Z.-Z. Yu, Woodhead Publishing Ltd., Cambridge, 2006.
- 32 J. Jordan, K. I. Jacob, R. Tannenbaum, M. A. Sharaf and I. Jasiuk, *Mater. Sci. Eng., A*, 2005, **393**, 1.
- 33 Z. Han and A. Fina, *Prog. Polym. Sci.*, 2011, **36**, 914.
- 34 G. Choudalakis and A. D. Gotsis, *Eur. Polym. J.*, 2009, **45**, 967.
- 35 M. Rahmat and P. Hubert, *Compos. Sci. Technol.*, 2011, **72**, 72.
- 36 J.-P. Salvetat, G. A. D. Briggs, J.-M. Bonard, R. R. Basca, A. J. Kulik, T. Stöckli, N. A. Burnham and L. Forró, *Phys. Rev. Lett.*, 1999, **82**, 944.
- 37 T. W. Ebbesen, H. J. Lezec, H. Hiura, J. W. Bennett, H. F. Ghaemi and T. Thio, *Nature*, 1996, **382**, 54.
- 38 S. Berber, Y.-K. Kwon and D. Tomanek, *Phys. Rev. Lett.*, 2000, **84**, 4613.
- 39 L. Li, Y. Yang, G. Yang, X. Chen, B. S. Hsiao, B. Chu, J. E. Spanier and C. Y. Li, *Nano Lett.*, 2006, **6**, 1007.
- 40 L. Li, C. Y. Li and C. Ni, *J. Am. Chem. Soc.*, 2006, **128**, 1692.
- 41 G. Xy, Y. Zhuang, R. Xia, J. Cheng and Y. Zhang, *Mater. Lett.*, 2012, **89**, 272.
- 42 H. G. Chae, M. L. Minus and S. Kumar, *Polymer*, 2006, **47**, 3494.
- 43 M. Hegde, U. Lafont, B. Norder, S. J. Picjen, E. T. Samulski, M. Rubinstein and T. Dingemans, *Macromolecules*, 2013, **46**, 1492.
- 44 J. Kaur, J. H. Lee and M. L. Shofner, *Polymer*, 2011, **52**, 4337.
- 45 G. Allegra, G. Raos and M. Vacatello, *Prog. Polym. Sci.*, 2008, **33**, 683.
- 46 Q. H. Zheng, A. B. Yu and G. Q. Lu, *Prog. Polym. Sci.*, 2008, **33**, 191.
- 47 P. V. Komarov, Y.-T. Chiu, S.-M. Chen and P. Reineker, *Macromol. Theory Simul.*, 2010, **19**, 64.
- 48 B. Hess, C. Kutzner, D. van der Spoel and E. Lindahl, *J. Chem. Theory Comput.*, 2008, **4**, 435.
- 49 D. Van der Spoel, E. Lindahl, B. Hess, G. Groenhoff, A. E. Mark and H. J. C. Berendsen, *J. Comput. Chem.*, 2005, **26**, 1701.
- 50 C. Oostenbrink, A. Villa, A. E. Mark and W. F. van Gunsteren, *J. Comput. Chem.*, 2004, **25**, 1656.
- 51 S. V. Lyulin, S. V. Larin, A. A. Gurtovenko, A. V. Lyulin, V. M. Nazarychev, S. G. Falkovich, V. E. Yudin, V. M. Svetlichyi and I. V. Gofman, *Soft Matter*, 2014, submitted.
- 52 H. J. C. Berendsen, in *Computer Simulations in Material Science*, ed. M. Meyer and V. Pontikis, Kluwer, Dordrecht, 1991.
- 53 H. J. C. Berendsen, J. P. M. Postma, W. F. van Gunsteren, A. Dinola and J. R. J. Haak, *Chem. Phys.*, 1984, **81**, 3684.
- 54 H. J. C. Berendsen, J. P. M. Postma, W. F. van Gunsteren, A. DiNola and J. R. J. Haak, *J. Chem. Phys.*, 1984, **81**, 3684.
- 55 B. Hess, H. Bekker, H. J. C. Berendsen and J. G. E. M. Fraaije, *J. Comput. Chem.*, 1997, **18**, 1463.
- 56 A. V. Lyulin and M. A. J. Michels, *Macromolecules*, 2002, **35**, 1463.
- 57 A. V. Lyulin, N. K. Balabaev and M. A. J. Michels, *Macromolecules*, 2003, **36**, 8574.
- 58 S. Karanikas and I. G. Economou, *Eur. Polym. J.*, 2011, **47**, 735.
- 59 T. Mulder, V. A. Harmandaris, A. V. Lyulin, N. F. A. van der Vegt, B. Vorselaars and M. A. J. Michels, *Macromol. Theory Simul.*, 2008, **17**, 290.
- 60 B. Vorselaars, A. V. Lyulin and M. A. J. Michels, *J. Chem. Phys.*, 2009, **130**, 074905.
- 61 P. G. Khalatur, P. M. Pakhomov and A. S. Pavlov, *Polym. Sci. U.S.S.R.*, 1983, **25**, 1937.
- 62 H. L. Chen, C. L. Lee and C. L. Chen, *Polymer*, 1994, **35**, 5057.
- 63 Q. Liao and X. Jin, *J. Chem. Phys.*, 1999, **110**, 8835.
- 64 V. A. Harmandaris, V. G. Mavrantzas and D. N. Theodorou, *Macromolecules*, 1998, **31**, 7934.
- 65 S. Fujawara and T. Sato, *Phys. Rev. Lett.*, 1998, **80**, 991.
- 66 T. A. Kavassalis and P. R. A. Sundararajan, *Macromolecules*, 1993, **26**, 4144.
- 67 X. Zhang, Z. Li, Z. Lu and C. Sun, *Polymer*, 2002, **43**, 3223.
- 68 M. S. Lavine, N. Waheed and G. C. Rutledge, *Polymer*, 2003, **44**, 1771.
- 69 M. J. Ko, N. Waheed, M. S. Lavine and G. C. Rutledge, *J. Chem. Phys.*, 2004, **121**, 2823.
- 70 T. Yamamoto, *J. Chem. Phys.*, 2008, **129**, 184903.
- 71 H. Yang, Y. Chen, Y. Liu, W. S. Cain and Z. S. Li, *J. Chem. Phys.*, 2007, **127**, 0904902.
- 72 H. Yang, X. J. Zhao and M. Sun, *Phys. Rev. E: Stat., Nonlinear, Soft Matter Phys.*, 2011, **84**, 011803.
- 73 A. A. Granovsky, Firefly version 7.1.G, <http://classic.chem.msu.su/gran/firefly/index.html>.
- 74 T. Darden, D. York and L. Pedersen, *J. Chem. Phys.*, 1993, **98**, 10089.
- 75 U. Essmann, L. Perera, M. L. Berkowitz, T. Darden, H. Lee and L. G. Pedersen, *J. Chem. Phys.*, 1995, **103**, 8577.
- 76 D. N. Theodorou and U. W. Suter, *Macromolecules*, 1985, **18**, 1467.
- 77 D. N. Theodorou and U. W. Suter, *Macromolecules*, 1986, **19**, 139.
- 78 S. Neyertz, *Soft Mater.*, 2007, **4**, 15.
- 79 T. Mulder, V. A. Harmandaris, A. V. Lyulin, N. F. A. van der Vegt, K. Kremer and M. A. J. Michels, *Macromolecules*, 2009, **42**, 384.
- 80 S. Pandiyani, D. Brown, N. F. A. van der Vegt and S. Neyertz, *J. Polym. Sci., Part B: Polym. Phys.*, 2009, **47**, 1166.
- 81 D. Hofmann, L. Fritz, J. Ulbrich and D. Paul, *Comput. Theor. Polym. Sci.*, 2000, **10**, 419.
- 82 S. Neyertz and D. Brown, *J. Chem. Phys.*, 2001, **115**, 708.
- 83 G. D. Smith, R. L. Jaffe and D. Y. Yoon, *Macromolecules*, 1993, **26**, 298.

- 84 S. Y. Lim, M. Sahimi, T. T. Tsotsis and N. Kim, *Phys. Rev. E: Stat., Nonlinear, Soft Matter Phys.*, 2007, **76**, 011810.
- 85 J. Xia, S. Liu, P. K. Pallathadka, M. L. Chng and T. Chung, *Ind. Eng. Chem. Res.*, 2010, **49**, 12014.
- 86 D. Hofmann, M. Heuchel, Y. Yampolskii, V. Khotimskii and V. Shantarovich, *Macromolecules*, 2002, **35**, 2129.
- 87 M. Heuchel and D. Hofmann, *Desalination*, 2002, **144**, 67.
- 88 M. Heuchel, D. Hoffmann and P. Pullumbi, *Macromolecules*, 2004, **37**, 201.
- 89 T. Yamamoto, *Polymer*, 2009, **50**, 1975.
- 90 B. G. Sumpter, D. W. Noid, G. L. Liang and B. Wunderlich, *Adv. Polym. Sci.*, 1994, **116**, 27.
- 91 E. Oleinik, I. Karmilov, S. Shenogin, A. Kalashnikov, M. Mazo, N. Balabaev and S. Chvalun, *Macromol. Symp.*, 1999, **146**, 133.
- 92 H. M. Colquhoun and D. J. William, *Acc. Chem. Res.*, 2000, **33**, 189.
- 93 N. Metatla, S. Palato, B. Commarieu, J. P. Claverie and A. Soldera, *Soft Matter*, 2012, **8**, 347.
- 94 D. J. Bakon and N. A. Geary, *J. Mater. Sci.*, 1983, **18**, 853.
- 95 N. A. Romanos and D. N. Theodorou, *Macromolecules*, 2010, **43**, 5455.
- 96 T. L. Phillips and S. A. Hanna, *Polymer*, 2005, **46**, 11003.
- 97 N. Takahashi, M. Hikosaka and T. Yamamoto, *Physica B*, 1996, **219 & 220**, 420.
- 98 A. Minoia, L. Chen, D. Beljonne and R. Lazzaroni, *Polymer*, 2012, **53**, 5480.
- 99 C. J. Lee, *J. Macromol. Sci., Rev. Macromol. Chem. Phys.*, 1989, **29**, 431.
- 100 D. Hofmann, L. Fritz, J. Ulbrich, C. Schepers and M. Böhning, *Macromol. Theory Simul.*, 2000, **9**, 293.
- 101 G. Tsolou, G. V. Mavrantzas and D. N. Theodorou, *Macromolecules*, 2005, **38**, 1478.
- 102 S. Pandiyan, D. Brown, S. Neyertz and N. F. A. van der Vegt, *Macromolecules*, 2010, **43**, 2605.
- 103 E. Pinel, D. Brown, C. Bas, R. Mercier, N. D. Alberola and S. Neyertz, *Macromolecules*, 2002, **35**, 10198.
- 104 S. Neyertz, *Macromol. Theory Simul.*, 2007, **16**, 513.
- 105 A. Karantrasos, R. J. Composto, K. I. Winey and N. Clarke, *Macromolecules*, 2011, **44**, 9830.
- 106 S. Chakraborty and S. Roy, *J. Phys. Chem. B*, 2012, **116**, 3083.
- 107 D. Qi, J. Hinkley and G. He, *Modell. Simul. Mater. Sci. Eng.*, 2005, **13**, 493.
- 108 R. Rahman and A. Haque, *Composites, Part B*, 2013, **54**, 353.
- 109 D. N. Theodorou and U. W. Suter, *Macromolecules*, 1985, **18**, 1206.
- 110 D. Brown, P. Mélé, S. Marceau and N. D. Albérola, *Macromolecules*, 2003, **36**, 1395.
- 111 N. Peng, T. S. Chung, M. L. Chng and W. Aw, *J. Membr. Sci.*, 2010, **360**, 48.
- 112 A. Shavit and R. A. Riggelman, *Macromolecules*, 2013, **46**, 5044.